ACS Energy LETTERS

http://pubs.acs.org/journal/aelccp

LETTER

High-Performance Lithium Metal Negative Electrode with a Soft and Flowable Polymer Coating

Guangyuan Zheng,[†,◇,▽] Chao Wang,[‡,◇] Allen Pei,[†,◇] Jeffrey Lopez,[‡,◇] Feifei Shi,[†] Zheng Chen,[‡,○] Austin D. Sendek,[§] Hyun-Wook Lee,[†,◆] Zhenda Lu,[†,¶] Holger Schneider,[⊥] Marina M. Safont-Sempere,[⊥] Steven Chu,[∥,■] Zhenan Bao,*[,‡] and Yi Cui*[,†,#]

[†]Department of Materials Science and Engineering, [‡]Department of Chemical Engineering, [§]Department of Applied Physics, [∥]Department of Physics, and [■]Department of Molecular and Cellular Physiology, Stanford University, Stanford, California 94305, United States

[⊥]BASF SE, Ludwigshafen 67056, Germany

[#]Stanford Institute for Materials and Energy Sciences, SLAC National Accelerator Laboratory, Menlo Park, California 94025, United States

Supporting Information

ABSTRACT: The future development of low-cost, high-performance electric vehicles depends on the success of next-generation lithium-ion batteries with higher energy density. The lithium metal negative electrode is key to applying these new battery technologies. However, the problems of lithium dendrite growth and low Coulombic efficiency have proven to be difficult challenges to overcome. Fundamentally, these two issues stem from the instability of the solid electrolyte interphase (SEI) layer, which is easily damaged by the large volumetric changes during battery cycling. In this work, we show that when a highly viscoelastic polymer was applied to the lithium metal electrode, the morphology of the lithium deposition became significantly more uniform. At a high current density of 5 mA/cm^2 we obtained a flat and dense lithium metal layer, and we observed stable cycling Coulombic efficiency of ∼97% maintained for more than 180 cycles at a current density of 1 mA/cm^2.

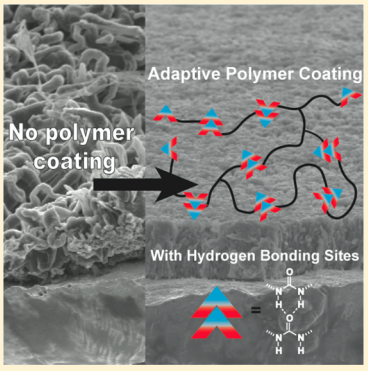

Improved battery technology is critical for the implementation of low-cost electric vehicles (EVs), which currently use batteries with a cost of around $400/kWh at the pack level.[1] To lower this cost and make EVs competitive with internal combustion engine vehicles, it is necessary to develop new electrode materials with high capacity and low cost such as lithium (Li) metal and silicon negative electrodes as well as sulfur and air positive electrodes.[2−7] Specifically, the Li metal negative electrode is a promising candidate for next-generation high-energy-density batteries because it has the highest theoretical specific capacity (3860 mAh/g) and the lowest potential of any negative electrode material for Li-based batteries.[8] Successful application of Li metal electrodes will fundamentally enable many advanced battery technologies (Li−S and Li−air) that can potentially offer specific energies 5−10 times greater than that of today's best lithium ion batteries and help reduce battery cost to meet the DOE target of <$150/kWh.[1,6]

Unfortunately, the problems of dendrite growth and low Coulombic efficiency (CE) have prevented Li metal electrodes from commercialization. A critical challenge for ensuring high performance of Li metal electrodes is the formation of a stable, uniform solid electrolyte interphase (SEI) layer on the Li surface that can withstand the large volumetric change during cycling.[1,9−11] Local variations in the SEI layer composition can lead to nonuniform deposition of Li due to changes in Li-ion conductivity across the electrode or breakage of the SEI (Figure 1a). These SEI defects facilitate the growth of high-surface area Li dendrites that increase electrolyte decomposition and cause the accumulation of dead Li, leading to increased impedance and capacity loss. The resulting dendrites can also eventually grow through the battery separator causing short-circuiting[2−7,12] and thermal runaway.[8,13]

Previous approaches to prevent lithium dendrite growth include modifying electrolyte formulations[1,6,14−17] and using electrolyte additives to improve morphology through the formation of a soft SEI,[18] addition of lithium halides,[19−22] or introducing electrostatically shielding layers.[23] The effect of

Received: September 19, 2016
Accepted: November 14, 2016
Published: November 14, 2016

DOI: 10.1021/acsenergylett.6b00456
ACS Energy Lett. 2016, 1, 1247−1255

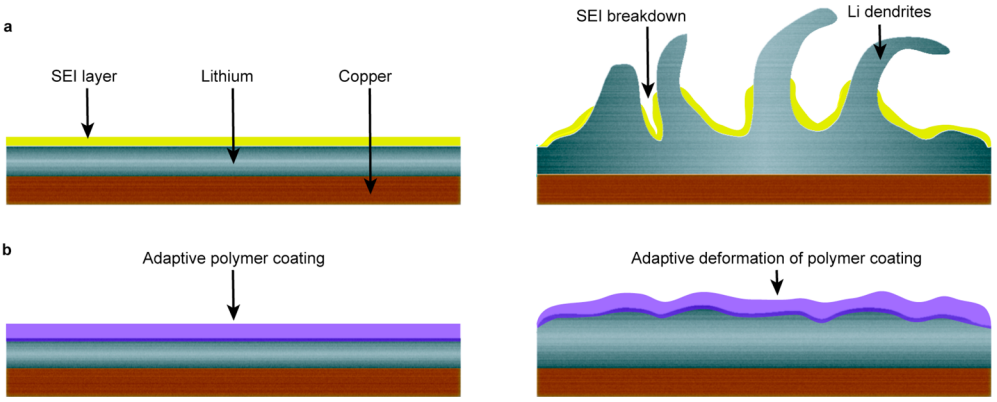

Figure 1. Schematic diagrams of lithium deposition. (a) Growth of lithium dendrites is usually observed for deposition on a bare electrode. (b) With the polymer coating, the highly adaptive polymer provides conformal coating onto the lithium metal electrode.

these additives on improving lithium deposition was observed at relatively low current densities (0.1−0.5 mA/cm^2). Other approaches focus on mechanically suppressing the dendrites after formation with cross-linked[24] or high modulus[25,26] polymer separators/electrolytes. Alternatively, bulk host materials have shown promise in addressing the issue of large volume changes in the lithium metal negative electrode.[27−30] For dendrite-free electrodes at high current densities, we have previously demonstrated that interfacial engineering allows for uniform deposition of lithium metal at a current density of around 1 mA/cm^2.[31,32] However, high current densities of 3 mA/cm^2 and above are usually desired. Such high current cycling usually puts more strain on the interfacial stability of the lithium metal electrode, and preventing cracking of the SEI layer demands a more innovative approach.

Here, we demonstrate a method to improve the Li metal cycling at high current densities by using a soft polymer coating on the electrode. The polymer used here is highly viscoelastic, which provides a pinhole-free coating on the Li surface during repeated charging and discharging. We hypothesize that the slow flow of the polymer across the electrode surface prevents the formation of cracks or pinholes in the SEI layer, inhibiting dendrite formation by avoiding the creation of "hot spots" where lithium ion flux is dramatically increased (Figure 1b). Our simulation indicates that when a pinhole or SEI defect is repaired, the reduced ionic conductivity of the polymer compared to that of the liquid electrolyte serves to homogenize the local current density and suppress the amplification of lithium growth. With our polymer coating, uniform Li deposition is achieved at high current densities of 5 mA/cm^2. The dendrite-free deposition of lithium metal also leads to extended electrochemical cycling and stable CE.

The polymer we use here was previously reported to exhibit self-healing properties[33] and was used to successfully enable Si negative electrodes in Li-ion batteries.[34] We slightly modified the synthesis to make materials on a larger scale with less batch-to-batch variations using a mechanical stir rod and a controlled reaction atmosphere of dry air. The first step consists of a condensation reaction between branched oleic acids and diethylene triamine to obtain the polymer backbone. This intermediate product is then reacted with a controlled amount of urea to produce a viscoelastic material that is highly stretchable because of the presence of the weaker hydrogen bonding cross-links in the structure (Figure 2a). The polymer structure is confirmed using NMR (Figure S1). In order for the flow to occur on a reasonable time scale, the polymer chains must be mobile so that the bonding groups can spontaneously rearrange. Our polymer has been designed to have a low T_g, measured around −26 °C, so that this process can occur at room temperature (Figure 2b). To further characterize the viscoelasticity of the polymer, oscillatory frequency sweep and stress relaxation experiments were carried out. The polymer shows typical viscoelastic behavior at 1% strain over a frequency range of 0.01−100 Hz (Figure 2c). The loss modulus (G''), or liquidlike characteristics, of the material dominate at low and intermediate frequencies until the crossover point near 1 Hz where the storage modulus (G') becomes higher and the material transitions to more solidlike behavior at short time scales. Rheological testing after swelling the polymer in electrolyte for 24 h shows that these viscoelastic properties do not change significantly in the presence of electrolyte solution and can be well-maintained even in the flooded environment of the coin cell (Figure S2). Stress relaxation experiments illustrate the highly liquidlike bulk properties of the material with quick and complete relaxation occurring very quickly after less than 10 s (Figure S3). This fully plastic deformation comes from the fast rearrangement of the hydrogen bonding groups that create the polymer structure. To illustrate the polymer's stretchability, we coat the polymer onto a stainless steel mesh and push the polymer through the mesh with a needle (Figure 2d). The optical images show that the polymer is highly stretchable even under the large local strains provided by the high aspect ratio needle.

The rheological properties of the polymer are highly sensitive to the amount of urea (and thus hydrogen bonding groups) used in the reaction (Figure S4), but the battery performance is found to be fairly insensitive to these variations in mechanical properties and shows similar cycling performance and electrochemical properties for polymer coatings synthesized with various reactant ratios (Figure S11). This is in agreement with previous studies showing that variations in the mechanical properties of this polymer have only a secondary effect on the cycling performance of silicon electrodes[35] and makes our material more versatile by providing a wide processing window in which to work. Additionally, we did find that the absorption of water into the polymer is a critical parameter affecting polymer-modified electrode performance. Because of the large number of hydrogen bonding groups in the polymer structure, it is very hygroscopic and absorbs noticeable amounts of water in air over the course of a few days. Water has a plasticizing effect on the viscoelastic polymer (Figures S3 and S4), but more importantly, it leads to poor electrochemical perform-

DOI: 10.1021/acsenergylett.6b00456
ACS Energy Lett. 2016, 1, 1247−1255

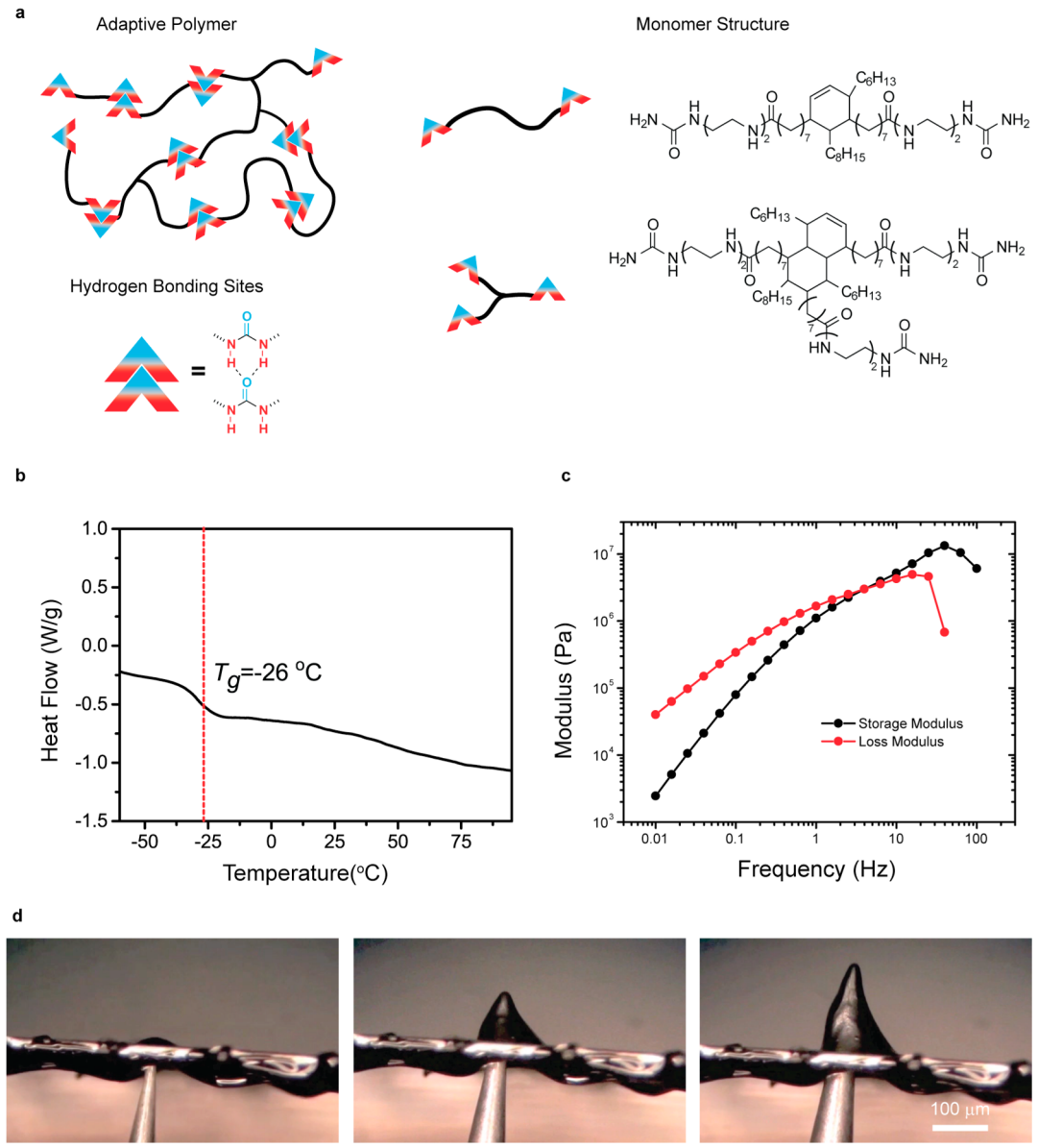

Figure 2. Physical properties of the polymer. (a) Chemical structure of the polymer. Black lines are the fatty acid backbone, and the red−blue boxes are the urea hydrogen-bonding sites. The right-hand side shows the molecular structure of the diacid and triacid backbones. (b) Differential scanning calorimetry (DSC) curve of the polymer showing that the T_g of polymer is around −26 °C, much lower than room temperature. (c) Frequency sweep measurement of the polymer showing the viscoelastic properties of the polymer. (d) Mechanical piercing of the polymer. The polymer is first laminated onto a stainless steel mesh. A needle controlled by a micromanipulator is then pushed onto the polymer. The figure shows that the viscoelastic polymer can withstand the needle without breaking.

ance. Compared to the materials that were rigorously dried (as reported in Experimental Methods), the wet polymer samples show reduced cycling lifetimes and unstable Coulombic efficiencies. Even so, keeping the polymer dry is readily achievable in most scenarios and does not diminish the promise of this approach.

For electrochemical testing of the soft polymer coating on lithium metal electrode we spin coat a thin layer (4 μm, as measured using profilometry) onto the copper (Cu) current collector. To study the effect of polymer on the lithium deposition, the morphology was examined using scanning electron microscopy (SEM). The electrodes were assembled in 2032 coin cells with lithium metal as both the reference and counter electrode, and Li was deposited on the polymer-modified electrodes at a current of 1 mA/cm^2. The electrolyte was 1 M lithium bis(trifluoromethanesulphonyl)imide (LiTFSI) in 1,3-dioxolane and 1,2-dimethoxyethane (volume ratio 1:1) with 1 wt % lithium nitrate ($LiNO_3$). Figure 3a−c shows the morphology of the Li on the polymer-modified and control (bare Cu) electrode. The large volumetric expansion of lithium deposition is known to cause breakdown of the SEI, resulting in localized areas of high lithium ion flux and corresponding growth of dendrites. The fresh surface of the dendritic lithium is immediately passivated by the electrolyte with a new SEI layer, preventing the lithium from closely packing together. As expected with 1 mAh/cm^2 of lithium deposited, the resulting structure on the control electrode shows a highly porous morphology (Figure 3a), which significantly increases the surface area of the Li metal and consumes more Li and electrolyte in undesirable side reactions.

DOI: 10.1021/acsenergylett.6b00456
ACS Energy Lett. 2016, 1, 1247−1255

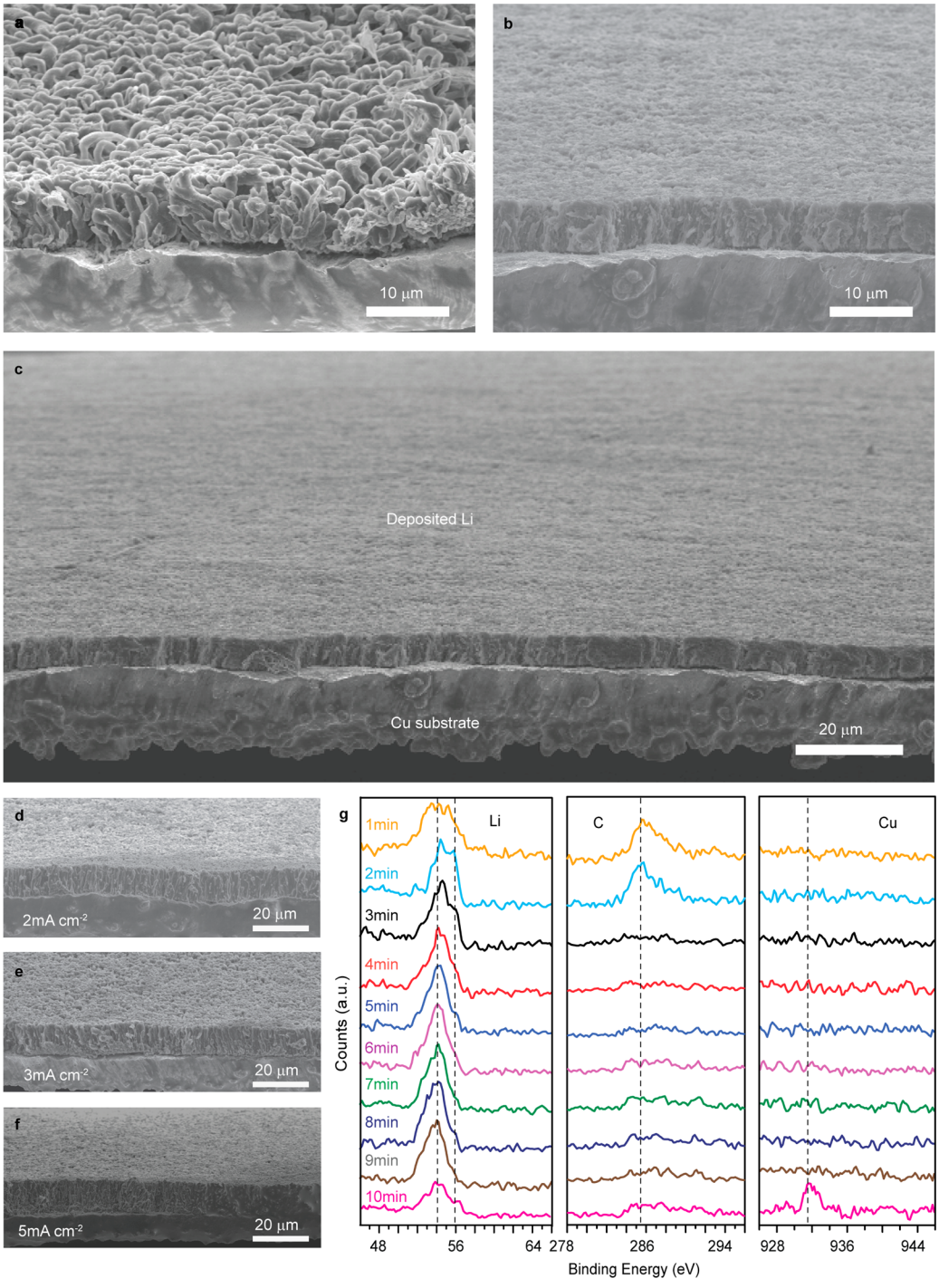

Figure 3. Characterization of lithium deposition. SEM images of 1 mAh/cm^2 of lithium deposited at 1 mA/cm^2 on (a) a bare copper electrode and (b) the polymer-modified electrode. (c) A lower-magnification image of panel b showing a large area of uniform deposition. SEM images of 2 mAh/cm^2 of lithium deposited at (d) 2 mA/cm^2, (e) 3 mA/cm^2, and (f) 5 mA/cm^2. (g) XPS spectra of lithium deposition with depth profiling.

On the other hand, deposition of lithium onto the modified electrode resulted in a much smoother and uniform morphology (Figure 3b,c). The highly viscoelastic polymer forms a uniform coating onto the lithium metal upon deposition and serves as a protecting layer that is soft and highly stretchable. It is interesting to note that the thickness of lithium deposition on the polymer-modified electrode is 5.1 μm, which is close to its theoretical value of around 5 μm for 1 mAh/cm^2 of Li. This suggests that the deposited lithium metal has low porosity, a desirable result of dense lithium metal deposition. The polymer coating is not observed in the SEM images because of the limitations of the ex situ measurements. Upon disassembling the cells, a significant portion of the polymer coating sticks to the separator, and more could be washed off when the electrode is rinsed during sample preparation. To eliminate the effect of the compression pressure of coin cell assembly in the resulting lithium morphology, we carried out the lithium deposition experiment

DOI: 10.1021/acsenergylett.6b00456
ACS Energy Lett. 2016, 1, 1247−1255

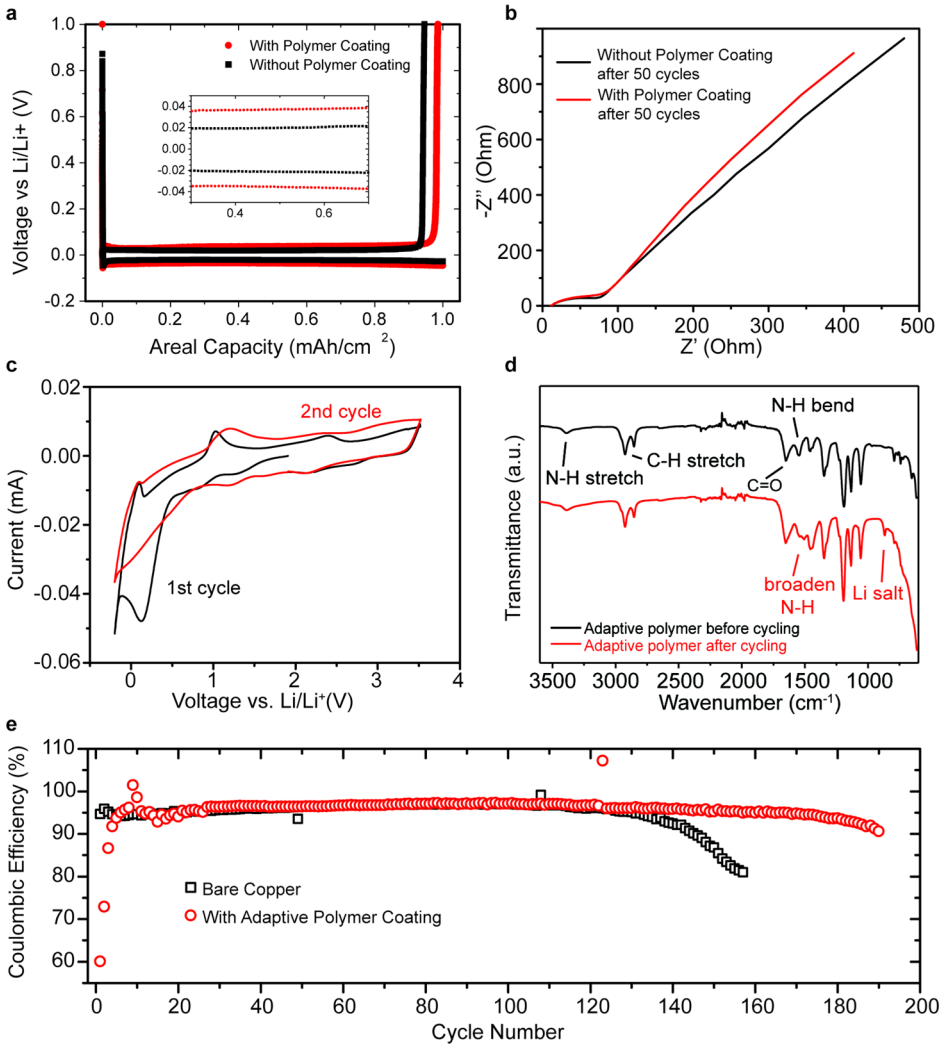

Figure 4. Electrochemical characterization of the electrodes. (a) Lithium deposition−dissolution voltage profiles from the 10th cycle shown for the polymer-coated electrode and control electrode. (b) Impedance spectra of the two electrodes after 50 cycles of lithium deposition and stripping. (c) Cyclic voltammetry of the polymer-modified electrode at a scan rate of 10 mV/s in a coin cell geometry with lithium metal as the reference and counter electrode. (d) FTIR spectra of the polymer before cycling and after 1 cycle of charge−discharge. (e) Cycling Coulombic efficiency of the lithium metal electrode with and without the polymer modification at a capacity of 1 mAh/cm^2.

in a pouch cell. The resulting lithium morphology is similar to that in a coin cell, confirming the effectiveness of the soft polymer coating in improving the lithium deposition behavior, with none of the pores or rough, filamentary Li seen on the control electrode present (Figure S5). The effect of uniform lithium deposition is consistently observed even at higher current density and high areal capacity. Panels d, e, and f of Figure 3 show the morphology of 2 mAh/cm^2 of deposited lithium at 2, 3, and 5 mA/cm^2, respectively.

This uniformity in lithium deposition is observed even at the beginning of lithium nucleation. When only a small amount of lithium (0.1 mAh/cm^2) is deposited, the lithium nuclei on the control electrode are relatively dispersed, forming large particles. On the other hand, lithium nucleation on the electrode modified with the polymer is relatively uniform and evenly distributed (Figure S6). The difference in the initial lithium nucleation phenomenon is probably due to the modification of the lithium metal with the polymer layer, which slightly reduces the lithium ion mobility adjacent to the lithium surface. The increased deposition overpotential resulting from the impedance of the polymer film produces smaller nuclei with increased areal nuclei density,[36,37] which ultimately grow to form the highly uniform, dense Li metal.

To study the spatial distribution of the polymer and lithium metal, we carried out X-ray photoelectron spectroscopy (XPS) with Ar ion sputtering on the electrode after lithium deposition. From the spectra (Figure 3g), we can see that the top of the sample shows signals of both lithium and carbon. The lithium signal from the top of the electrode shows both Li metal and Li salts (54 eV[15] and 56 eV,[38] respectively). The electrode was then sputtered with 5 kV Ar$^+$ ions to remove thin layers of the structure. After 2 min of sputtering, the carbon signal is substantially smaller. The lithium signal attributed to lithium salts at 56 eV also decreases, and only the lithium metal signal is observed. These observations indicate that the polymer forms a hybrid SEI containing Li salts and likely other decomposition products of the DOL/DME electrolyte. After 9 min of sputtering, the copper signal is observed, indicating that all of the polymer and Li has been removed. The slight lithium signal at the bottom of the electrode could be due to the residual lithium metal left behind during sputtering.

DOI: 10.1021/acsenergylett.6b00456
ACS Energy Lett. 2016, 1, 1247−1255

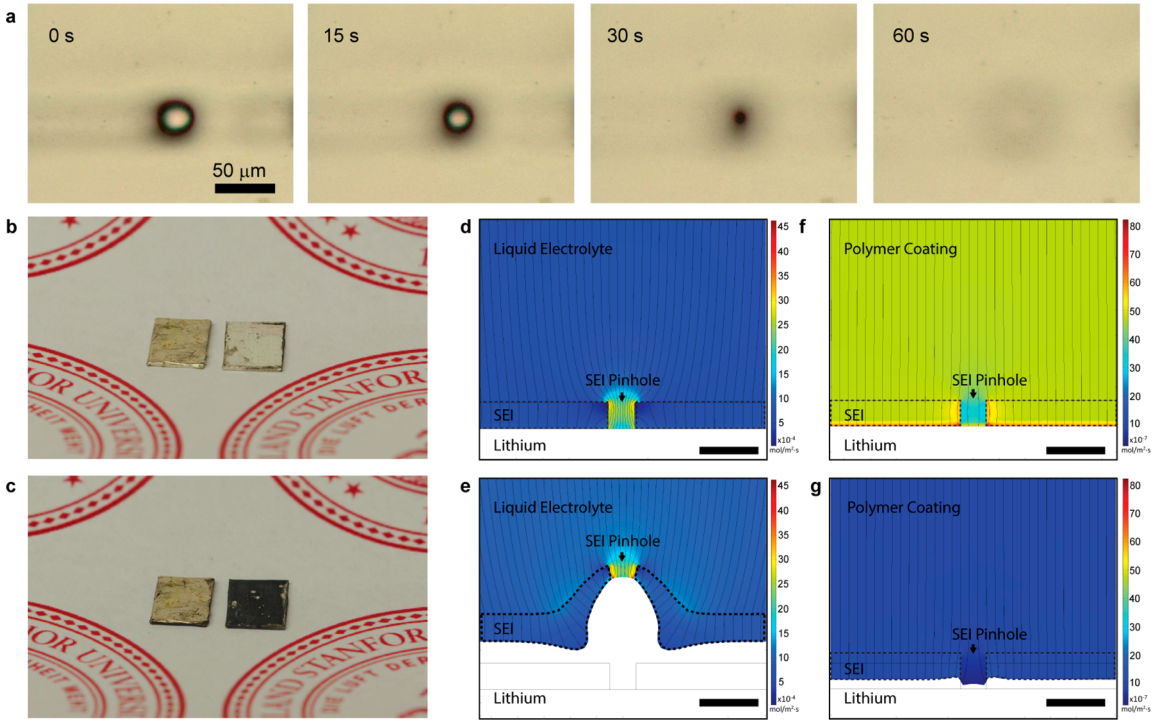

Figure 5. Pinhole-free polymer coating. (a) Optical microscope images showing the flowability of the polymer coating via the healing process of an artificially created pinhole. (b, c) Digital camera images showing the effect of pinhole-free coating of polymer on the lithium metal foil. The lithium foil on the left side is coated with polymer, and the right side is the control lithium foil. The images show the air stability of the polymer-coated lithium foil before (b) and after (c) 30 min of exposure to the ambient air. (d, e) Numerical simulation of the evolution of lithium dendrite growth in the case where a pinhole is created on the lithium SEI layer. Dendrite growth is clearly observed at the cracked location (e). (f, g) Numerical simulation of the effect of polymer coating on the lithium metal electrode, in the case in which an identical pinhole is created. Dendrite growth is significantly suppressed with the polymer coating (g). Scale bars: 400 nm.

The effect of the soft polymer coating on battery performance is also investigated through electrochemical testing. Galvanostatic cycling of lithium deposition and stripping was carried out on electrodes with and without the flowable polymer coating. The overpotential for lithium deposition and stripping for cells with the polymer is slightly higher than for those without, at −36 and −20 mV, respectively (Figure 4a). This is to be expected because the polymer has an ionic conductivity in the swollen state that is lower than that of the pure liquid electrolyte solution. The swollen state ionic conductivity of this polymer has been previously measured to be on the order of 10^{-4} S/cm.[35] Impedance measurement after 50 cycles also shows similar charge-transfer resistance between the two electrodes (Figure 4b). The stability of the polymer coating is examined with cyclic voltammetry and Fourier transform infrared (FTIR) spectra. The cyclic voltammetry shows that slight oxidation/reduction is observed at around 0.1−0.15 V during the first cycle (Figure 4c). For subsequent cycles, no significant reaction was observed in the voltage window between 0−1 V, which is the voltage range that the lithium deposition and dissolution processes are carried out. The FTIR spectra also confirms that the majority of the functional groups within the polymer are preserved after cycling. There is slight broadening of the N−H band, which could be due to reactions that took place during the initial cycling or slight interference of the electrolyte molecules or SEI products with the hydrogen bonding structure (Figure 4d). Detailed FTIR and XPS analyses of the SEI after 50 cycles of deposition and stripping further suggest that the polymer coating is stable during cycling (Figures S7−S9). The comparison of cycling performance of the electrodes shows significant improvement in the lithium deposition and dissolution when the soft polymer coating is present. Figure 4e shows that with the polymer coating, the Coulombic efficiency can be maintained at almost 97% for over 180 cycles at 1 mA/cm^2 current density. The average CE for the control electrode from cycle 20 to 100 is 96.4%, which is similar to that of the polymer-coated electrodes, but drops below 90% after 145 cycles. Polymer-coated electrodes with higher amounts of deposited lithium (3 mAh/cm^2) also exhibited enhanced performance compared to bare control electrodes, maintaining an average CE of over 97.7% for over 80 cycles, whereas the control electrode CE drops below 80% after just 75 cycles (Figure S13). We observed consistent performance for all of the electrodes that we prepared, showing that our fabrication method is quite robust (Figure S14).

The effectiveness of the polymer in improving the morphology of lithium deposition may be related to the conformal coating of the polymer on lithium. The viscoelasticity of the polymer means that any pinhole or inhomogeneity in the polymer coating will disappear quickly. Figure 5a shows the healing process of an artificially created pinhole in the polymer coating. Within 1 min, a pinhole with diameter of around 30 μm self-heals completely at room temperature. The pinhole-free polymer coating is also evidenced from its ability to provide stability to the lithium metal when in air. When bare lithium metal is exposed to the air, rapid reactions between lithium and atmospheric nitrogen, oxygen, and water vapor take place.[39] The surface of the unprotected lithium metal turns black within 30 min (Figure 5c). On the other hand, the

DOI: 10.1021/acsenergylett.6b00456
ACS Energy Lett. 2016, 1, 1247−1255

polymer allows the lithium metal foil to remain almost unchanged in the air over this same time period (Figure 5b,c). We hypothesize that the pinhole-free polymer coating ensures uniform lithium ion flux during deposition and protects the Li surface from emerging hotspots or SEI breakage.

This hypothesis is verified by the COMSOL simulation, which models the change in lithium deposition morphology with and without the soft polymer coating. Figure 5d,e shows the case where a pinhole is placed in the SEI of the flat lithium metal. The simulation results show that upon deposition, lithium metal quickly grows if no coating is present from the pinhole because of the reduction in resistance and subsequent amplified local ionic flux. With the polymer coating, the lithium deposition is found to be still uniform even if there is a defect on the native SEI layer. The COMSOL simulation details are discussed in Figure S15. An additional biased random walk simulation demonstrated the importance of the polymer ionic conductivity in encouraging uniform lithium deposition (Figure S16). These results suggest the unique advantages of the polymer in maintaining uniform deposition of lithium metal.

In conclusion, the present demonstration of a functional soft, viscoelastic polymer coating for improving Li metal electrodeposit morphology and electrochemical cycling represents a stark, but promising, deviation from conventional understanding. It has been reported that high modulus coatings or interfaces are effective for suppressing dendrite growth.[25,26,31,32] However, in this case it is not mechanical stiffness but rather the extreme softness and intrinsic polymer flow that are utilized to improve electrode uniformity. Our strategy of applying a thin protective coating directly to the electrode surface is straightforward and scalable. The viscoelastic and flow properties of the coating impart a homogenizing effect on Li^+ ion flux to prevent rapid dendrite formation at hotspots in the SEI. The present work highlights the importance of the design of a surface coating in enabling stable lithium metal negative electrodes that will suppress dendrite formation. With uniform lithium deposition even at high current densities up to 5 mA/cm^2 and improved electrochemical cycling performance, this work introduces a strategy that is counter to the idea that high modulus coatings are required for stable cycling of Li metal electrodes. Furthermore, other types of viscoelastic and supramolecular materials could also be potential candidates for modifying lithium metal to achieve improved cycling performance.

EXPERIMENTAL METHODS

Synthesis of Soft Polymer Coating. The design and synthesis of the self-healing polymer is a modified approach from previous reports.[33,34] We controlled the amount of urea and reaction time so that only part of the amine groups was converted into urea, yielding a polymer that is able to flow at room temperature without addition of any plasticizer. First, a mixture of diacid and triacid (Empol 1016, 41.5 g, donated by Cognis) was mixed with diethylenetriamine (17 g) at 120 °C for 2 h. Then the temperature was increased to 160 °C, and the reaction proceeded for 24 h with a constant flow of N_2 gas at 30 mL/min under a water-jacketed condenser. The product was dissolved in 100 mL of chloroform and washed three times with 75 mL of a methanol and water (1:2) solution to remove excess amine. The chloroform and residual water were removed via rotary evaporation at 40 °C and then 80 °C to obtain a randomly branched oligomer terminated with amine groups (M-NH_2). M-NH_2 (10 g) was reacted with 1 g of urea for 4 h at 135 °C under constant flow of dry air (50 mL/min) to obtain our viscoelastic polymer coating. The reaction mixture was stirred using a Trubore stirrer assembly (Ace Glass) to maintain a controlled atmosphere inside the reaction vessel. The polymer was then baked overnight at 80 °C under vacuum to remove trapped gas bubbles and water. The polymer was then immediately dissolved in a 1:1 chloroform and ethanol solution to limit the uptake of moisture from the atmosphere.

Electrochemical Testing. Electrochemical properties of the lithium metal electrodes were tested in 2032 coin cells with a 96-channel battery tester (Arbin Instruments). The working electrodes consisted of either a 1 cm^2 bare copper current collector or a Cu foil disc coated with the designed polymer. To coat the copper current collector, the polymer was dissolved in a 1:1 chloroform and ethanol solution at a concentration of 250 mg/mL. Solutions were passed through a 0.45 μm PTFE filter to remove any particulates before spin coating at 4000 rpm. After spin coating the electrodes were baked overnight at 50 °C under vacuum to remove any residual solvent. The counter electrode was Li metal foil (750 μm thick, Alfa Aesar) punched into a disc with area 0.5 cm^2. The electrolyte was 1 M lithium bis(trifluoromethanesulphonyl)imide (LiTFSI) in 1,3-dioxolane and 1,2-dimethoxyethane (volume ratio 1:1) with 1 wt % lithium nitrate ($LiNO_3$).[40] A commercially available polymer separator (Celgard 2325) was used between the two electrodes. The electrolyte (75 μL) was added to each cell to standardize the tests. The Coulombic efficiency measurement was carried out by depositing 1 mAh cm^{-2} (unless otherwise noted) of lithium onto the working electrode followed by stripping to 1 V. Cycling tests were carried out by first depositing a fixed amount of Li onto the electrode, followed by Li stripping up to 1 V. Coulombic efficiency is calculated by dividing the amount of lithium stripped over the amount of lithium deposited during each cycle. Cycling tests were initialized by cycling the electrodes between 0 and 1 V for 10 cycles. Electrochemical impedance spectroscopy measurements were taken over a frequency range of 200 mHz to 1 MHz. Impedance and cyclic voltammetry measurements were taken using a potentiostat (Biologic).

Material Characterization. NMR (1H) spectra were recorded on a Varian Mercury 400 MHz NMR spectrometer at room temperature. FTIR spectra were measured using a Nicolet iS50 FT/IR Spectrometer (Thermo Fisher) with a diamond attenuated total reflectance (ATR) attachment. Rheological experiments were carried out using an Ares G2 Rheometer (TA Instruments) with an advanced Peltier system (APS) at 25 °C as the bottom geometry and a 25 mm parallel plate as the top geometry. The gap height was 1 mm. Frequency sweeps were carried out from 0.1 to 100 Hz at 1% strain, and stress relaxation experiments were performed at 1% strain. Differential scanning calorimetry (DSC) experiments were performed using a DSC-Q2000 (TA Instruments) over a temperature range of −70 to 150 °C with a ramp rate of 10 °C/min. T_g data was taken from the second heating cycle. X-ray photoelectron spectroscopy (XPS) spectra were measured with a PHI 5000VersaProbe system with an Al Kα radiation (1486 eV) source. A FEI XL30 Sirion SEM with FEG source was used for SEM characterizations

Simulation. The COMSOL Tertiary Nernst−Planck Electrodeposition module with deforming geometry was used to simulate the effects of a polymer coating over a pinhole on the Li surface. The ionic current distribution and the Li metal surface geometry change was simulated as Li deposition was

DOI: 10.1021/acsenergylett.6b00456
ACS Energy Lett. 2016, 1, 1247−1255

carried out on the bare and polymer-modified electrode surfaces. Further simulation parameters and details can be found in the Supporting Information.

■ ASSOCIATED CONTENT

Supporting Information

The Supporting Information is available free of charge on the ACS Publications website at DOI: 10.1021/acsenergylett.6b00456.

NMR spectra, rheological characterization, SEM images, FTIR and XPS characterization of the SEI, additional electrochemical cycling data, and simulation details (PDF)

■ AUTHOR INFORMATION

Corresponding Authors

*E-mail: zbao@stanford.edu.

*E-mail: yicui@stanford.edu.

ORCID

Allen Pei: 0000-0001-8930-2125

Present Addresses

▽G.Z.: Institute of Materials Research and Engineering, 2 Fusionopolis Way, Innovis #08-03, Singapore 138634.

○Z.C.: Department of NanoEngineering, University of California, San Diego, La Jolla, CA 92093.

◆H.-W.L.: School of Energy and Chemical Engineering, Ulsan National Institute of Science and Technology (UNIST), Ulsan 44919, Republic of Korea.

¶Z.L.: College of Engineering and Applied Science, Nanjing University, Nanjing 210093, China.

Author Contributions

◇G.Z., C.W., A.P., and J.L. contributed equally to this work.

Notes

The authors declare no competing financial interest.

■ ACKNOWLEDGMENTS

We acknowledge the support from the Assistant Secretary for Energy Efficiency and Renewable Energy, Office of Vehicle Technologies of the U.S. Department of Energy through the Advanced Battery Materials Research (BMR) Program (Battery500 Consortium). This work was also supported by BASF through the California Research Alliance (CARA). Part of this work was performed at the Stanford Nano Shared Facilities (SNSF). G.Z. acknowledges financial support from the Agency for Science, Technology and Research (A*STAR), Singapore. A.P. acknowledges the support from the U.S. Department of Defense through the National Defense Science & Engineering Graduate Fellowship (NDSEG) Program and from Stanford University through the Stanford Graduate Fellowship (SGF) Program. J.L. acknowledges support by the National Science Foundation Graduate Research Fellowship Program under Grant DGE-114747. A.D.S. acknowledges funding from the Stanford University Office of Technology Licensing Fellowship through the Stanford Graduate Fellowship program.

■ REFERENCES

(1) Nykvist, B.; Nilsson, M. Rapidly Falling Costs of Battery Packs for Electric Vehicles. *Nat. Clim. Change* **2015**, *5*, 329−332.

(2) Chu, S.; Majumdar, A. Opportunities and Challenges for a Sustainable Energy Future. *Nature* **2012**, *488*, 294−303.

(3) Armand, M.; Tarascon, J. M. Building Better Batteries. *Nature* **2008**, *451*, 652−657.

(4) Chan, C. K.; Peng, H.; Liu, G.; McIlwrath, K.; Zhang, X. F.; Huggins, R. A.; Cui, Y. High-Performance Lithium Battery Anodes Using Silicon Nanowires. *Nat. Nanotechnol.* **2008**, *3*, 31−35.

(5) Scrosati, B.; Garche, J. Lithium Batteries: Status, Prospects and Future. *J. Power Sources* **2010**, *195*, 2419−2430.

(6) Bruce, P. G.; Freunberger, S. A.; Hardwick, L. J.; Tarascon, J.-M. Li-O2 and Li-S Batteries with High Energy Storage. *Nat. Mater.* **2012**, *11*, 19−29.

(7) Sun, Y.; Liu, N.; Cui, Y. Promises and Challenges of Nanomaterials for Lithium-Based Rechargeable Batteries. *Nat. Energy* **2016**, *1*, 16071.

(8) Xu, W.; Wang, J.; Ding, F.; Chen, X.; Nasybulin, E.; Zhang, Y.; Zhang, J.-G. Lithium Metal Anodes for Rechargeable Batteries. *Energy Environ. Sci.* **2014**, *7*, 513−537.

(9) Aurbach, D.; Cohen, Y. Morphological Studies of Li Deposition Processes in $LiAsF_6$/PC Solutions by in Situ Atomic Force Microscopy. *J. Electrochem. Soc.* **1997**, *144*, 3355−3360.

(10) Aurbach, D.; Zinigrad, E.; Cohen, Y.; Teller, H. A Short Review of Failure Mechanisms of Lithium Metal and Lithiated Graphite Anodes in Liquid Electrolyte Solutions. *Solid State Ionics* **2002**, *148*, 405−416.

(11) Li, Z.; Huang, J.; Liaw, B. Y.; Metzler, V.; Zhang, J. A review of lithium deposition in lithium-ion and lithium metal secondary batteries. *J. Power Sources* **2014**, *254*, 168−182.

(12) Finegan, D. P.; Scheel, M.; Robinson, J. B.; Tjaden, B.; Hunt, I.; Mason, T. J.; Millichamp, J.; Di Michiel, M.; Offer, G. J.; Hinds, G.; et al. In-Operando High-Speed Tomography of Lithium-Ion Batteries During Thermal Runaway. *Nat. Commun.* **2015**, *6*, 6924.

(13) von Sacken, U.; Nodwell, E.; Sundher, A.; Dahn, J. R. Comparative Thermal Stability of Carbon Intercalation Anodes and Lithium Metal Anodes for Rechargeable Lithium Batteries. *J. Power Sources* **1995**, *54*, 240−245.

(14) Crowther, O.; West, A. C. Effect of Electrolyte Composition on Lithium Dendrite Growth. *J. Electrochem. Soc.* **2008**, *155*, A806−A811.

(15) Suo, L.; Hu, Y.-S.; Li, H.; Armand, M.; Chen, L. A New Class of Solvent-in-Salt Electrolyte for High-Energy Rechargeable Metallic Lithium Batteries. *Nat. Commun.* **2013**, *4*, 1481.

(16) Park, M. S.; Ma, S. B.; Lee, D. J.; Im, D.; Doo, S.-G.; Yamamoto, O. A Highly Reversible Lithium Metal Anode. *Sci. Rep.* **2014**, *4*, 3815.

(17) Qian, J.; Henderson, W. A.; Xu, W.; Bhattacharya, P.; Engelhard, M.; Borodin, O.; Zhang, J.-G. High Rate and Stable Cycling of Lithium Metal Anode. *Nat. Commun.* **2015**, *6*, 6362.

(18) Mogi, R.; Inaba, M.; Jeong, S.-K.; Iriyama, Y.; Abe, T.; Ogumi, Z. Effects of Some Organic Additives on Lithium Deposition in Propylene Carbonate. *J. Electrochem. Soc.* **2002**, *149*, A1578−A1583.

(19) Hirai, T.; Yoshimatsu, I.; Yamaki, J.-I. Effect of Additives on Lithium Cycling Efficiency. *J. Electrochem. Soc.* **1994**, *141*, 2300−2305.

(20) Kanamura, K.; Shiraishi, S.; Takehara, Z.-I. Electrochemical Deposition of Very Smooth Lithium Using Nonaqueous Electrolytes Containing HF. *J. Electrochem. Soc.* **1996**, *143*, 2187−2197.

(21) Ishikawa, M.; Kawasaki, H.; Yoshimoto, N.; Morita, M. Pretreatment of Li Metal Anode with Electrolyte Additive for Enhancing Li Cycleability. *J. Power Sources* **2005**, *146*, 199−203.

(22) Lu, Y.; Tu, Z.; Archer, L. A. Stable Lithium Electrodeposition in Liquid and Nanoporous Solid Electrolytes. *Nat. Mater.* **2014**, *13*, 961−969.

(23) Ding, F.; Xu, W.; Graff, G. L.; Zhang, J.; Sushko, M. L.; Chen, X.; Shao, Y.; Engelhard, M. H.; Nie, Z.; Xiao, J.; et al. Dendrite-Free Lithium Deposition via Self-Healing Electrostatic Shield Mechanism. *J. Am. Chem. Soc.* **2013**, *135*, 4450−4456.

(24) Khurana, R.; Schaefer, J. L.; Archer, L. A.; Coates, G. W. Suppression of Lithium Dendrite Growth Using Cross-Linked Polyethylene/Poly(Ethylene Oxide) Electrolytes: a New Approach for Practical Lithium-Metal Polymer Batteries. *J. Am. Chem. Soc.* **2014**, *136*, 7395−7402.

(25) Stone, G. M.; Mullin, S. A.; Teran, A. A.; Hallinan, D. T.; Minor, A. M.; Hexemer, A.; Balsara, N. P. Resolution of the Modulus Versus

DOI: 10.1021/acsenergylett.6b00456
ACS Energy Lett. 2016, 1, 1247−1255

Adhesion Dilemma in Solid Polymer Electrolytes for Rechargeable Lithium Metal Batteries. *J. Electrochem. Soc.* **2012**, *159*, A222−A227.
(26) Tung, S.-O.; Ho, S.; Yang, M.; Zhang, R.; Kotov, N. A. A Dendrite-Suppressing Composite Ion Conductor From Aramid Nanofibres. *Nat. Commun.* **2015**, *6*, 6152.
(27) Liu, Y.; Lin, D.; Liang, Z.; Zhao, J.; Yan, K.; Cui, Y. Lithium-Coated Polymeric Matrix as a Minimum Volume-Change and Dendrite-Free Lithium Metal Anode. *Nat. Commun.* **2016**, *7*, 10992.
(28) Yan, K.; Lu, Z.; Lee, H.-W.; Xiong, F.; Hsu, P.-C.; Li, Y.; Zhao, J.; Chu, S.; Cui, Y. Selective Deposition and Stable Encapsulation of Lithium Through Heterogeneous Seeded Growth. *Nat. Energy* **2016**, *1*, 16010.
(29) Liang, Z.; Lin, D.; Zhao, J.; Lu, Z.; Liu, Y.; Liu, C.; Lu, Y.; Wang, H.; Yan, K.; Tao, X.; et al. Composite Lithium Metal Anode by Melt Infusion of Lithium Into a 3D Conducting Scaffold with Lithiophilic Coating. *Proc. Natl. Acad. Sci. U. S. A.* **2016**, *113*, 2862−2867.
(30) Lin, D.; Liu, Y.; Liang, Z.; Lee, H.-W.; Sun, J.; Wang, H.; Yan, K.; Xie, J.; Cui, Y. Layered Reduced Graphene Oxide with Nanoscale Interlayer Gaps as a Stable Host for Lithium Metal Anodes. *Nat. Nanotechnol.* **2016**, *11*, 626−632.
(31) Zheng, G.; Lee, S. W.; Liang, Z.; Lee, H.-W.; Yan, K.; Yao, H.; Wang, H.; Li, W.; Chu, S.; Cui, Y. Interconnected Hollow Carbon Nanospheres for Stable Lithium Metal Anodes. *Nat. Nanotechnol.* **2014**, *9*, 618−623.
(32) Yan, K.; Lee, H.-W.; Gao, T.; Zheng, G.; Yao, H.; Wang, H.; Lu, Z.; Zhou, Y.; Liang, Z.; Liu, Z.; et al. Ultrathin Two-Dimensional Atomic Crystals as Stable Interfacial Layer for Improvement of Lithium Metal Anode. *Nano Lett.* **2014**, *14*, 6016−6022.
(33) Cordier, P.; Tournilhac, F.; Soulié-Ziakovic, C.; Leibler, L. Self-Healing and Thermoreversible Rubber From Supramolecular Assembly. *Nature* **2008**, *451*, 977−980.
(34) Wang, C.; Wu, H.; Chen, Z.; McDowell, M. T.; Cui, Y.; Bao, Z. Self-Healing Chemistry Enables the Stable Operation of Silicon Microparticle Anodes for High-Energy Lithium-Ion Batteries. *Nat. Chem.* **2013**, *5*, 1042−1048.
(35) Lopez, J.; Chen, Z.; Wang, C.; Andrews, S. C.; Cui, Y.; Bao, Z. The Effects of Cross-Linking in a Supramolecular Binder on Cycle Life in Silicon Microparticle Anodes. *ACS Appl. Mater. Interfaces* **2016**, *8*, 2318−2324.
(36) Sano, H.; Sakaebe, H.; Senoh, H.; Matsumoto, H. Effect of Current Density on Morphology of Lithium Electrodeposited in Ionic Liquid-Based Electrolytes. *J. Electrochem. Soc.* **2014**, *161*, A1236−A1240.
(37) Sagane, F.; Ikeda, K.; Okita, K.; Sano, H.; Sakaebe, H. Effects of Current Densities on the Lithium Plating Morphology at a Lithium Phosphorus Oxynitride Glass Electrolyte/Copper Thin Film Interface. *J. Power Sources* **2013**, *233*, 34−42.
(38) Aurbach, D.; Pollak, E.; Elazari, R.; Salitra, G.; Kelley, C. S.; Affinito, J. On the Surface Chemical Aspects of Very High Energy Density, Rechargeable Li−Sulfur Batteries. *J. Electrochem. Soc.* **2009**, *156*, A694−A702.
(39) Markowitz, M. M.; Boryta, D. A. Lithium Metal-Gas Reactions. *J. Chem. Eng. Data* **1962**, *7*, 586−591.
(40) Li, W.; Yao, H.; Yan, K.; Zheng, G.; Liang, Z.; Chiang, Y.-M.; Cui, Y. The Synergetic Effect of Lithium Polysulfide and Lithium Nitrate to Prevent Lithium Dendrite Growth. *Nat. Commun.* **2015**, *6*, 7436.

DOI: 10.1021/acsenergylett.6b00456
ACS Energy Lett. 2016, 1, 1247−1255